PHILOSOPHICAL TRANSACTIONS OF THE ROYAL SOCIETY A

Phil. Trans. R. Soc. A (2005) **363**, 565–573
doi:10.1098/rsta.2004.1508
Published online 5 January 2005

Kinetic equivalence of the heat and cold structural transitions of $\lambda_{6–85}$

By Wei Y. Yang† and Martin Gruebele

Center for Biophysics and Computational Biology, and Departments of Chemistry and Physics, University of Illinois, Urbana, IL 61801, USA (gruebele@scs.uiuc.edu)

Heat- and cold-denatured proteins are considered separate thermodynamic states because temperature tuning requires the protein to pass through two 'soft' first-order phase transitions. When both pressure and temperature changes are allowed, the heat- and cold-denatured states of proteins can be interconverted without going through the native state. This raises the question of whether these states are distinguished from one another by their folding kinetics. For the Tyr22-Trp/Ala37Gly/Ala49Gly mutant of the 80 residue five-helix bundle protein $\lambda_{6–85}$, we show that viscosity-corrected folding rates do not distinguish the cold- and heat-denatured states. We attribute this to a folding mechanism dominated by hydrophobic collapse. Our 'temperature-symmetric' approach offers an alternative to viscosity tuning with solvent additives in such cases.

Keywords: cold denaturation; heat denaturation; pressure denaturation; phase transition; temperature jump; kinetics

1. Introduction

The cold denaturation, pressure denaturation and heat denaturation transitions of proteins are analogous to macroscopic first-order phase transitions. They involve a latent heat (Privalov *et al*. 1971; Privalov & Khechinashvili 1974; Royer 2002) and they occur over a narrow range of the thermodynamic parameter being tuned (typically 5–20 °C or 1000 bar). Since the classic work of Hawley (1971) it has been known that the joint temperature–pressure dependence of the free energy must be described at least by a parabolic function.

This immediately suggests another analogy with macroscopic phase transitions, such as the boiling of water. There, the first-order transition from vapour to liquid can be avoided by first compressing the vapour above the critical pressure, then cooling it to below the critical temperature, and then decompressing the fluid. Figure 1 shows a P–T phase diagram for a typical protein. The cold- and heat-denatured states

† Present address: Division of Engineering and Applied Sciences, Harvard University, Cambridge, MA 02138, USA.

One contribution of 17 to a Discussion Meeting 'Configurational energy landscapes and structural transitions in clusters, fluids and biomolecules'.

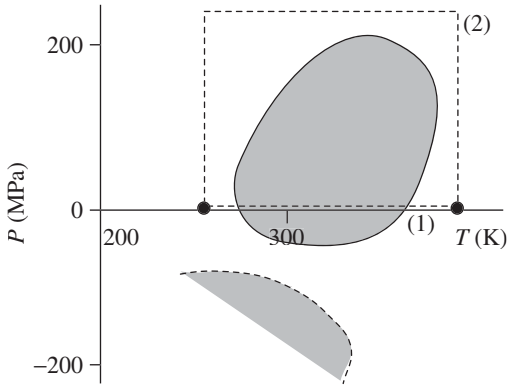

Figure 1. Phase diagram for protein folding, showing the quadratic region of stability. We postulate there may be an additional stabilizing region caused by drying (ten Wolde & Chandler 2002) at negative pressures (shown shaded), but it is not known whether this lies below the homogeneous nucleation point where the solvent cavitates. The (1) ordinary and (2) phase-transition free paths between the heat- and cold-denatured states are shown.

are usually connected by two 'soft' first-order phase transitions via the folded state. ('Soft' here means that a finite-sized system, such as a protein, has a narrow, but not sharp, transition region.) We also show a path (2), which connects the heat- and cold-denatured states, which are usually considered to be separate thermodynamic states, without going through any first-order phase transitions.

Such a conversion among heat- and cold-denatured states via a high-pressure state raises the question of how the heat- and cold-denatured states are distinguished from one another. Radii of gyration, heat capacity changes, fluorescence changes, or even line distributions in nuclear magnetic resonance (NMR) spectra, have not proven to be reliable guides (Damaschun *et al*. 1993; Ervin *et al*. 2002; Huang & Oas 1996; Privalov 1990; Sabelko *et al*. 1998). Especially for small apparent two-state proteins, the difference between the heat and cold denatured states becomes small because both lack any significant buried hydrophobic surfaces. The main difference comes from the residual preference for their secondary structures.

One might expect folding kinetics to be a more sensitive distinguishing property between these states (Nash *et al*. 1996). For example, changes from non-exponential to exponential folding kinetics, as the temperature of phosphoglycerate kinase is lowered, have been attributed to a decrease of energy landscape roughness in the cold-denatured state, which does not occur in the heat-denatured state (Sabelko *et al*. 1999).

In this paper, we show that the folding kinetics from cold- and heat-denatured states of a small 5-helix bundle are identical within measurement uncertainty, if a correction for solvent viscosity is made. We examine the folding/unfolding kinetics of a variant of $\lambda_{6\text{–}85}$ (figure 2). The relaxation rate is highly sensitive to the addition of even small amounts of denaturants. On the other hand, the relaxation rates corrected for viscosity are identical for relaxation between the native state and either the cold- or heat-denatured states, as long as experiments are compared at identical folding free energies. This opens up the possibility of temperature tuning as an alternative approach to adjusting the solvent viscosity without additives such as sugars.

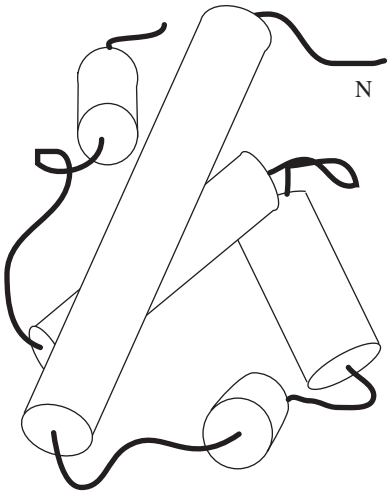

Figure 2. Topology of the λ_{6-85} five-helix bundle used in this work, with the N-terminus indicated.

2. Samples and measurement methods

The λ repressor N-terminal domain gene (residues 6–85) was inserted into the PET-15b vector (Novagen) between the NdeI and BamHI cutting sites, allowing histidine–nickel binding-based purification. Wild-type lambda repressor is too stable to cold denature in the absence of denaturant, and lacks a tryptophan to be used for fluorescence detection of the kinetics (Burton *et al*. 1997; Ghaemmaghami *et al*. 1998). We engineered the point mutations Tyr22Trp, Ala37Gly and Ala49Gly into the protein with the Quickchange site-directed mutagenesis kit (Stratagene) (Hecht *et al*. 1984). This reduced the stability sufficiently to allow cold denaturation. Proteins were expressed in Rosetta (DE3) pLysS (Novagen) cells, as described previously. Harvested cells were lysed by passing them through a French press twice at more than 12 000 psi†, and λ-repressor was purified from the soluble fraction. Purification on an Ni–NTA column (Qiagen) with imidazole as the eluting reagent was followed by a size-exclusion column, such as a Sephacryl S-200 HR column (Amershan Pharmacia) at pH 8, 20 mM Tris and 500 mM NaCl. Histidine tags were removed with thrombin (Novagen), as described previously. Pure protein was dialysed extensively against water and lyophilized for storage at −20 °C. Low-resolution electrospray ionization mass spectrometry was used to confirm the triple mutation. Protein concentration was estimated using 280 nm absorption of the protein solution assuming that the extinction coefficient of 5600 $\mathrm{cm}^{-1}\,\mathrm{M}^{-1}$ for trytophans and 1300 $\mathrm{cm}^{-1}\,\mathrm{M}^{-1}$ for tyrosines (Edelhoch 1967). All measurements were in 50 mM potassium phosphate buffer at pH 7.

Cold and heat denaturation were verified by circular dichroism at 222 nm on a JASCO J-715 equipped with a Peltier temperature controller. Cold and heat denaturation were further verified by fluorescence spectra excited at 280 nm and collected with a 385 nm longpass filter on the same instrument. Extruded fused silica cuvettes

† 1 psi ≈ 7 kPa.

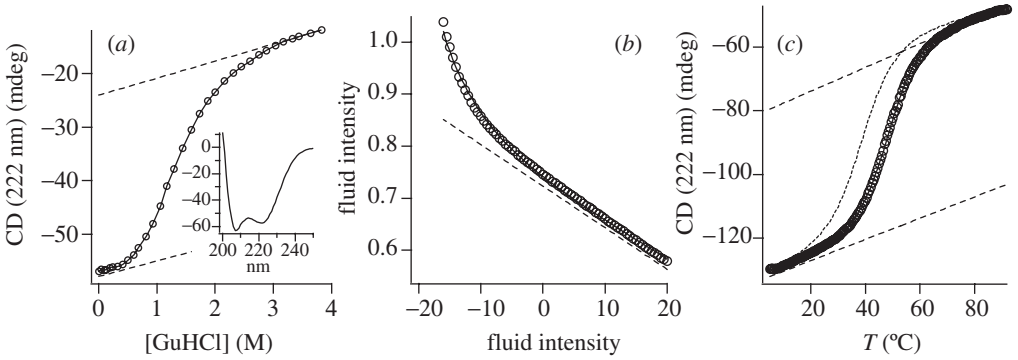

Figure 3. (*a*) GuHCl denaturation curve of $\lambda_{6\text{–}85}$ at 20 °C; insert: native CD spectrum at 20 °C without denaturant. (*b*) Cold denaturation in the absence of denaturant measured by fluorescence. (*c*) Heat denaturation in absence of denaturant and in 0.5 M guanidine hydrochloride (dotted curve) measured by circular dichroism. In all cases, the smooth curve through the data is from the simultaneous fit to equation (3.1), and dotted straight lines are fitted baselines. The protein concentration was *ca.* 5 μM.

were used for measurements in supercooled water to −15 °C. A native CD spectrum in the 200–250 nm range at 20 °C was also obtained.

Relaxation kinetics were induced by a 10 ns Neodymium:YAG heating pulse, Raman shifted to 1.54 μm in 30 MPa of methane (Ballew *et al.* 1996). *T*-jump sizes at different temperatures were matched to equalize the initial and final equilibrium constants. The use of extruded silica cuvettes made possible *T*-jumps in supercooled solution for the cold-denaturation measurements. Folding/unfolding relaxation was probed by a 14 ns-spaced pulse train of 280 nm light from a frequency-tripled Ti:sapphire laser, exciting the tryptophan in the fluorescent mutant. The time evolution of the tryptophan fluorescence spectrum, imaged by a monochromator onto a 16 channel photomultiplier array, was used to track the protein folding kinetics, as described previously (Ervin *et al.* 2000). For the relatively slow folding ($\tau > 150$ μs) mutant discussed here, only single exponential kinetics were observed, as predicted (Yang & Gruebele 2004*a*).

3. Results

The native CD spectrum of the mutant is very close in shape to the pseudo-wild type containing the tyrospine → tryptophan mutation, but 8% smaller at 222 nm (figure 3 insert; Ghaemmaghami *et al.* (1998)) This slight loss of signal is due to a small amount of denatured protein present even at room temperature (see fitting below, accounts for *ca.* 4%), and the two alanine → glycine substitutions, which slightly reduce helix content.

The CD signal at 222 nm, and the fluorescence pumped at 280 nm, were obtained on a grid of 0, 0.125, 0.25 and 0.5 M GuHCl, and of −15 to 80 °C in 0.5 °C increments, and for a guanidine hydrochloride titration from 0 to 3.8 M at 20 °C. To illustrate the data, figure 3 shows the guanidine hydrochloride titration detected by circular dichroism, the cold denaturation detected by fluorescence and the heat denaturation detected by circular dichroism at 222 nm.

Table 1. *Thermodynamic parameters for the cold and heat denaturation of* $\lambda_{6\text{–}85}$ Y22W/A37G/A49G

parameter	value
T_0	287.5 ± 2 K
ΔG_0	-7.4 ± 0.2 kJ mol^{-1}
ΔG_2	$0.006\,54 \pm 0.000\,02$ kJ mol^{-1} K^{-2}
m	4.2 ± 0.04 kJ mol^{-1} M^{-1}
ΔG_m	0.149 ± 0.002 kJ mol^{-1}M^{-1} K^{-1}

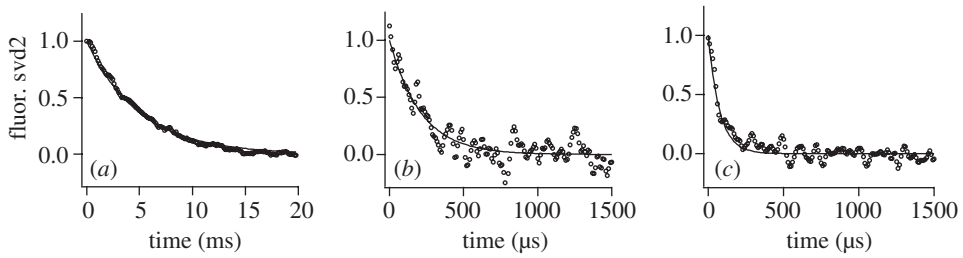

Figure 4. (*a*) Relaxation kinetics from the cold-denatured state in presence of 0.5 M guanidine hydrochloride denaturant ($T = 3\,^\circ$C, $\tau = 4.98 \pm 0.6$ ms). (*b*) Relaxation from the cold-denatured state without denaturant ($T = 4.7\,^\circ$C, $\tau = 210 \pm 15$ µs). (*c*) Relaxation to the heat-denatured state without denaturant ($T = 34\,^\circ$C, $\tau = 75 \pm 8$ µs). Both kinetic traces have nearly identical equilibrium constants as endpoints. All measurements at pH 7, 57 ± 3 µM protein concentration. Fluor.svd2: second singular value decomposition component of the raw fluorescence data.

The data can be reproduced within measurement uncertainty by a very simple model. The free energy of folding is represented by a Taylor series in the guanidine hydrochloride concentration and temperature,

$$\Delta G(T) = \Delta G_0 + \Delta G_2 (T - T_0)^2 + m[\mathrm{GuHCl}] + \Delta G_\mathrm{m}[\mathrm{GuHCl}](T - T_0), \qquad (3.1)$$

where T_0 is the temperature of highest stability, and the quadratic expansion in T is required to obtain both cold and heat denaturation. The temperature-denaturant cross term ΔG_m accounts for the small shift in the temperature of maximal stability in the presence of denaturant. All 476 denaturation data points were fitted simultaneously to equation (3.1). We tested more complicated three-state and heat capacity models, without any improvement over the fits shown in figure 3. The model provides an accurate description of the temperature and guanidine hydrochloride denaturation curves over the range from -15 to $60\,^\circ$C (figure 3). Most importantly, the temperature of highest stability is accurately represented. Thus, relative equilibrium constants as a function of $T - T_0$ are accurate, even if errors in ΔG_0 cause the absolute equilibrium constants to be off by a scale factor. The fitting parameters with uncertainties are shown in table 1.

Figure 4 shows the temperature-jump relaxation of $\lambda_{6\text{–}85}$ between the cold-denatured and native states in 0.5 M guanidine hydrochloride. The fitted relaxation rate is 5200 ± 100 µs. We also compared the rates for two T-jumps probing cold-denatured-native and heat-denatured–native transitions ($-4.7/34\,^\circ$C). The initial and final temperatures were chosen so that equilibration occurs between nearly identical pairs of equilibrium constants. Under these conditions, the ratio of relaxation

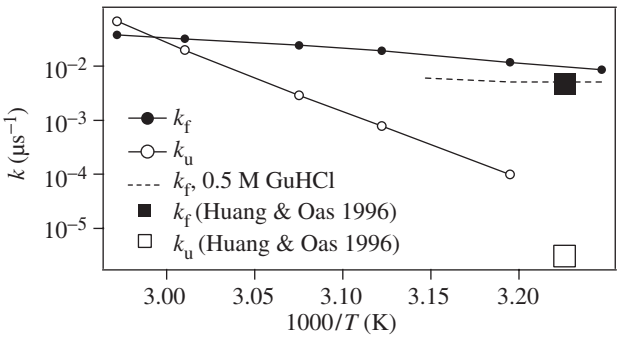

Figure 5. Heat-denatured $\longleftrightarrow$ native folding and unfolding rates of $\lambda_{6\text{–}85}$ as a function of temperature, and the extrapolated rate obtained by Oas and co-workers from NMR line width measurements in denaturant. The observed rate exceeds the extrapolated rate.

rates is the same as the ratio of folding rates. (The assumption of two-state folding that has to be made for further analysis has been verified in reference (Yang & Gruebele 2004*a*) for this mutant.) The results for the $-4.7/34\,^{\circ}\mathrm{C}$ pair are shown in figure 4 ($210 \pm 15\,\mu\mathrm{s}$ from the cold-denatured state, $75 \pm 8\,\mu\mathrm{s}$ to the heat-denatured state). All relaxations were much faster than those observed in dilute guanidinium buffer.

Heat-denaturation relaxation rates for $\lambda_{6\text{–}85}$ were collected over a wide range of temperatures, and for [GuHCl] = 0, 0.125, 0.25 and 0.5 M. The folding and unfolding rates were obtained by fitting the T-jump induced relaxation k_{obs} to a single exponential decay at each temperature, and using the equilibrium constant $K(T)$ to compute the folding and unfolding rate constants according to

$$\left.\begin{aligned} k_{\mathrm{f}}(T) &= \frac{k_{\mathrm{obs}}(T)K(T)}{1+K(T)}, \\ k_{\mathrm{u}}(T) &= \frac{k_{\mathrm{obs}}(T)}{1+K(T)}. \end{aligned}\right\} \tag{3.2}$$

Unlike some of the very fast folding variants of $\lambda_{6\text{–}85}$, the triple mutant exhibited no deviations from single exponential kinetics. Figure 5 shows the folding and unfolding rates obtained at different temperatures, and also the extrapolated folding rates at 37 °C from high-denaturant NMR line width measurements obtained by Oas and co-workers (Huang & Oas 1996).

4. Discussion

Comparison of the relaxation rates from the cold-denatured states with those from the heat-denatured states in figure 4 indicates that they are kinetically equivalent, as follows: the model in table 1 predicts that $\Delta G \approx -4.9 \pm 0.2\,\mathrm{kJ\,mol^{-1}}$ at both $-4.7\,^{\circ}\mathrm{C}$ and $34\,^{\circ}\mathrm{C}$. To an excellent approximation

$$\frac{k_{\mathrm{obs}}^{\mathrm{heat}}}{k_{\mathrm{obs}}^{\mathrm{cold}}} = \frac{k_{\mathrm{f}}^{\mathrm{heat}}}{k_{\mathrm{f}}^{\mathrm{cold}}}$$

must therefore hold. The kinetics in figure 4 yield a ratio of relaxation rates of 2.8 ± 0.4, the lower temperature relaxation being slower. For two-state kinetics in

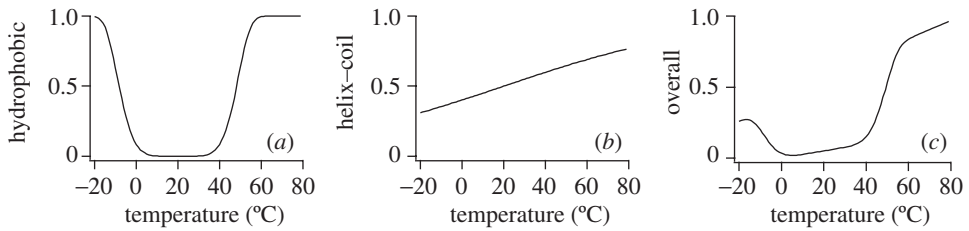

Figure 6. Symmetry and asymmetry in heat and cold denaturation: 1, all denatured; 0, all folded. A simple model superimposes (*a*) a symmetrical re-entrant phase transition correlated with hydrophobicity and heat capacity, and (*b*) a non-cooperative helix–coil transition to yield (*c*) the slightly asymmetric cold- and heat-denaturation transition actually observed (cf. figure 3).

the Kramers overdamped regime, we have

$$\frac{k_1}{k_2} = \frac{\nu(\eta(T_1))\,\mathrm{e}^{-\Delta G^{+}(T_1)/kT_1}}{\nu(\eta(T_2))\,\mathrm{e}^{-\Delta G^{+}(T_2)/kT_2}}. \tag{4.1}$$

The relevant viscosities of water are 2.18 ± 0.05 cP at $-4.7\,^{\circ}$C and 0.75 ± 0.02 cP at $34\,^{\circ}$C, $\eta_1/\eta_2 \approx 2.9 \pm 0.1$. The ratio of the viscosities alone already accounts for the observed rate ratio. Thus $\Delta G^{\dagger}(-4.7\,^{\circ}\mathrm{C}) \approx \Delta G^{\dagger}(34\,^{\circ}\mathrm{C})$ and the barriers for refolding from cold- and heat-denatured states are indeed identical within measurement uncertainty.

Cold and heat denaturation are 'symmetrical' processes for this mutant of $\lambda_{6\text{–}85}$ as far as the folding barrier height is concerned. This similarity between the two states has also been observed for the Tyr22Trp mutant in denaturants using NMR (Huang & Oas 1996). Why do kinetics not distinguish the subtle differences between the two ensembles? Our explanation is that in our mutant the hydrophobic effect controls the barriers, and that for this small helical bundle the two unfolded ensembles are identical in terms of its exposed hydrophobic surfaces. We recently showed (Yang & Gruebele 2004*b*), by examining 15 mutants of $\lambda_{6\text{–}85}$, that they can be grouped into two broad classes: one set of molecules has a turnover in the folding rate (Gly-containing ones), while the others (Ala-containing ones) have anti-Arrhenius folding behaviour. This was attributed to a competition between hydrophobic contact formation, which should follow the strength of the hydrophobic effect and have a turnover at intermediate temperatures, and secondary structure formation, which was greatly enhanced at lower temperatures in the Alanine-containing molecules. The triple mutant considered here falls into the limit of destabilized secondary structure, so collapse controls the formation of the native state. On the other hand, we expect that mutants obeying anti-Arrhenius folding behaviour will have heat- and cold-denatured ensembles distinguishable by their folding rates.

The issue of how close to equivalent the heat- and cold-denatured ensembles are is related to a simple model that combines hydrophobic contact formation and the temperature dependence of the helix–coil transition has recently been put forward by H. Kihara and co-workers (2004, personal communication). It can be interpreted as shown schematically in figure 6. Collapse due to hydrophobicity is symmetric with respect to the temperature of highest collapse propensity, and slows down equally at lower and higher temperatures. This yields a relatively symmetrical population profile for the cold- and heat-denatured states. The helix–coil transition is only weakly cooperative, and changes much more slowly as a function of temperature, with increasing

helix at low temperature. When the two are superimposed, an asymmetric denaturation profile is obtained. The relative contribution of these two effects determines the degree of asymmetry of the two phase transitions, and hence whether hydrophobicity or secondary structure formation controls the kinetics. It would be interesting to see a computational study of Ala-containing mutants, as we predict that the relaxation rates for the heat- and cold-denatured states will differ under thermodynamically equivalent conditions. Unfortunately, the stability of these mutants precludes any cold denaturation at temperatures that we can achieve experimentally (we tested several from Yang & Gruebele (2004*b*)).

For molecules like Gly-rich $\lambda_{6\text{–}85}$ mutants, simple temperature tuning can thus be used as an alternative to viscogenic agents. A temperature shift of *ca.* 40 °C across the point of maximum stability yields a change in the viscosity of *ca.* 3, which fully accounts for the observed change in the rate. Although by itself the experiment cannot differentiate between deviations from Kramer's overdamped regime (*assumed* in equation (4.1)) and a change in the barrier, such experiments are particularly attractive for comparison with full-atom, off-lattice or implicit solvent molecular dynamics simulations of folding, where addition of another solvent component is undesirable, whereas temperature tuning in the 250–350 K range is straightforward.

Figure 5 shows that our $\lambda_{6\text{–}85}$ triple mutant folds faster than the extrapolation from a Chevron plot at 37 °C based on the NMR/denaturant line-width measurements by Oas and co-workers (Burton *et al.* 1997). Thus their claim for fast folding holds up for this mutant, as for all the others we have examined. Instead of a roll-over of the rate as denaturant is removed, characteristic of intermediate formation, we observe a speed-up of the kinetics. This further supports the observation that two-state kinetics of the fastest-folding variants of $\lambda_{6\text{–}85}$ give way to downhill folding on a rough free energy landscape, rather than folding through a single intermediate, when the native state is stabilized by removal of denaturant (Yang & Gruebele 2003, 2004*a*). It is worth noting that the two types of models (folding on a rough free energy landscape versus folding through a well-defined intermediate) are actually closely related: the landscape model posits a hierarchy of many intermediates of varying depths, many very shallow (approximately $1kT$) (Onuchic *et al.* 1997), while three-state kinetics simply posits a single intermediate. Molecular dynamics simulations of fast-folding and slower folding variants of $\lambda_{6\text{–}85}$ by Luthey-Schulten and co-workers support the idea of five to ten local free energy minima along the native contact reaction coordinate Q.

This work was supported by National Science Foundation grant no. MCB 0316925 and by ACS-PRF grant no. 37333-AC7. The authors thank C. Austen Angell and Peter G. Wolynes for stimulating discussions, and P. F. McMillan and D. C. Clary for the invitation to contribute to this issue.

References

Ballew, R. M., Sabelko, J., Reiner, C. & Gruebele, M. 1996 A single-sweep, nanosecond time resolution laser temperature-jump apparatus. *Rev. Scient. Instrum.* **67**, 3694–3699.

Burton, R. E., Huang, G. S., Daugherty, M. A., Calderone, T. L. & Oas, T. G. 1997 The energy landscape of a fast-folding protein mapped by Ala → Gly substitutions. *Nat. Struct. Biol.* **4**, 305–310.

Damaschun, G., Damaschun, H., Gast, K., Misselwitz, R., Müller, J. J., Pfeil, W. & Zirwer, D. 1993 Cold denaturation-induced conformational changes in phosphoglycerate kinase from yeast. *Biochemistry* **32**, 7739–7746.

Edelhoch, H. 1967 Spectroscopic determination of tryptophan and tyrosine in proteins. *Biochemistry* **6**, 1948–1954.

Ervin, J., Sabelko, J. & Gruebele, M. 2000 Submicrosecond real-time fluorescence detection: application to protein folding. *J. Photochem. Photobiol. B* **54**, 1–15.

Ervin, J., Larios, E., Osvath, S., Schulten, K. & Gruebele, M. 2002 What causes hyperfluorescence: folding intermediates or conformationally flexible native states? *Biophys. J.* **83**, 473–483.

Ghaemmaghami, S., Word, J. M., Burton, R. E., Richardson, J. S. & Oas, T. G. 1998 Folding kinetics of a fluorescent variant of monomeric λ repressor. *Biochemistry* **37**, 9179–9185.

Hawley, S. A. 1971 Reversible pressure-temperature unfolding of chymotrypsinogen. *Biochemistry* **10**, 2436–2442.

Hecht, M. H., Sturtevant, J. M. & Sauer, R. T. 1984 Effect of single amino acid replacements on the thermal stability of the NH_2 terminal domain of phage lambda repressor. *Proc. Natl Acad. Sci. USA* **81**, 5685–5689.

Huang, G. S. & Oas, T. G. 1996 Heat and cold denatured states of monomeric λ repressor are thermodynamically and conformationally equivalent. *Biochemistry* **35**, 6173–6180.

Nash, D., Lee, B. & Jonas, J. 1996 Hydrogen-exchange kinetics in the cold denatured state of ribonuclease A. *Biochim. Biophys. Acta* **1297**, 40–48.

Onuchic, J. N., Luthey-Schulten, Z. & Wolynes, P. G. 1997 Theory of protein folding: the energy landscape perspective. *A. Rev. Phys. Chem.* **48**, 545–600.

Privalov, P. L. 1990 Cold denaturation of proteins. *Crit. Rev. Biochem. Mol. Biol.* **25**, 281–305.

Privalov, P. L. & Khechinashvili, N. N. 1974 A thermodynamic approach to the problem of stabilization of globular protein structure: a calorimetric study. *J. Mol. Biol.* **86**, 665–684.

Privalov, P. L., Khechinashvili, N. N. & Atanasov, B. P. 1971 Thermodynamic analysis of thermal transitions in globular proteins. I. Calorimetric study of ribotrypsinogen, ribonuclease and myoglobin. *Biopolymers* **10**, 1865–1890.

Royer, C. A. 2002 Revisiting volume changes in pressure-induced protein unfolding. *Biochim. Biophys. Acta* **1595**, 201–209.

Sabelko, J., Ervin, J. & Gruebele, M. 1998 The cold denatured ensemble of apomyoglobin: implications for the early steps of folding. *J. Phys. Chem. B* **102**, 1806–1819.

Sabelko, J., Ervin, J. & Gruebele, M. 1999 Observation of strange kinetics in protein folding. *Proc. Natl Acad. Sci. USA* **96**, 6031–6036.

ten Wolde, P. R. & Chandler, D. 2002 Drying-induced hydrophobic polymer collapse. *J. Mol. Biol.* **311**, 373–393.

Yang, W. Y. & Gruebele, M. 2003 Folding at the speed limit. *Nature* **423**, 193–197.

Yang, W. Y. & Gruebele, M. 2004*a* Folding lambda repressor at its speed limit. *Biophys. J.* **87**, 596–608.

Yang, W. Y. & Gruebele, M. 2004*b* Rate-temperature relationships in lambda repressor fragment 6–85 folding. *Biochemistry* **43**, 13 018–13 025.